**Iraqi National Journal of Earth Science**

www.earth.mosuljournals.com

# Geothermal Potential Assessment and Subsurface Structural Mapping of the Southern Bida Basin, Nigeria Using Aeromagnetic Dataset

**George-Best Azuoko[1], Ayatu Ojonugwa Usman [2*], Amobi Chigozie Ekwe [3]**

*[1,2,3] Department of Geology /Geophysics, Faculty of Physical Science, Alex Ekwueme Federal University, Ndufu-Alike, Ikwo, Ebonyi, Nigeria*

**Article information**

**Received:** 12- June -2024

**Revised:** 20- Jul -2024

**Accepted:** 20- Aug -2024

**Available online:** 01- Jul – 2025

**Keywords**:
Geothermal Gradient
Subsurface Structure
Sedimentary Pill
Spectral Analysis
Euler Deconvolution

**Correspondence:**
**Name:** Ayatu Ojonugwa Usman

Email: ayatuusman@gmail.com

## ABSTRACT

A magnetic dataset over some portions of the southern Bida Basin, Nigeria, has been evaluated using spectral analysis and Euler deconvolution techniques. The geothermal potentials and the subsurface structures of the region are delineated from the data. Qualitative assessment of the total magnetic intensity (TMI) and first vertical derivative maps of the region reveal evidence of intrusion around the northeastern and southeastern portions of the research area. The entire region is greatly faulted, with the major fault trending east west (E-W). The Euler deconvolution map reveals clusters of different rock bodies in contact with each other delineated as dyke and sill structures. These structures have depth range values between 01 and 1917 m. The results from the spectral analysis reveal two depth source models in the region, namely the high sedimentary pill region ranging from 1.79 to 3.30 km, and the low sedimentary pill region ranging from 0.41 to 1.45 km. The 3D real-view map of the sedimentary infilling within the mapped area shows that the sedimentary pills are undulating and structurally controlled within the research area. The geothermal gradient and the Curie isotherm depth are estimated to range from 19.10 to 32.10 °C/km, and this is not sufficient for geothermal energy exploitation. The current investigation has been able to pinpoint the igneous intrusive zones that should be avoided when investigating hydrocarbons. It also yields a model that makes identifying possible geologic structures that control magnetic ore mineral deposits in the region easier.

DOI: 10.33899/earth.2024.150856.1298, 

# تقييم الإمكانات الحرارية الأرضية ورسم خرائط تركيبية تحت سطحية لحوض بيدا الجنوبي، نيجيريا، باستخدام مجموعة بيانات مغناطيسية جوية

**جورج بيست أزوكو[1]، آياتو أوجونوغوا عثمان[*2]، أموبي تشيغوزي إيكوي [3]**

*[3،2،1] قسم الجيولوجيا / الجيوفيزياء، كلية العلوم الفيزيائية، جامعة ألكس إكويمي الفيدرالية، ندوفو-اليك، إيكو، إبوني، نيجيريا.*

**معلومات الارشفة**

**تاريخ الاستلام:** 12- يونيو -2024

**تاريخ المراجعة:** 20- يوليو -2024

**تاريخ القبول:** 20- أغسطس-2024

**تاريخ النشر الالكتروني:** 01- يوليو -2025

**الكلمات المفتاحية:**

التدرج الحراري الأرضي

البنية تحت السطحية

الكبسولة الرسوبية

التحليل الطيفي

تفكيك أويلر

**المراسلة:**

**الاسم:** آياتو أوجونوغوا عثمان

Email: ayatuusman@gmail.com

**الملخص**

تم تقييم مجموعة بيانات مغناطيسية تغطي بعض أجزاء حوض بيدا الجنوبي، نيجيريا، باستخدام التحليل الطيفي وتقنيات تفكيك أويلر. حُددت الإمكانات الحرارية الأرضية والتراكيب تحت السطحية للمنطقة من البيانات. يكشف التقييم النوعي لشدة المغناطيسية الكلية (TMI) وخرائط المشتق الرأسي الأول للمنطقة عن أدلة على وجود تداخل حول الأجزاء الشمالية الشرقية والجنوبية الشرقية من منطقة البحث. المنطقة بأكملها متصدعة بشدة، حيث يتجه الصدع الرئيسي من الشرق إلى الغرب (شرقًا-غربًا). تكشف خريطة تفكيك أويلر عن مجموعات من أجسام صخرية مختلفة متلامسة مع بعضها البعض، مُحددة على شكل تراكيب سد وعتبة. تتراوح قيم عمق هذه الهياكل بين 0.1 و1.917 مترًا. تكشف نتائج التحليل الطيفي عن نموذجين لمصادر العمق في المنطقة، وهما منطقة الرواسب الرسوبية العالية التي تتراوح بين 1.79 و3.30 كم، ومنطقة الرواسب الرسوبية المنخفضة التي تتراوح بين 0.41 و1.45 كم. تُظهر الخريطة ثلاثية الأبعاد للرواسب المتراكمة في المنطقة المرسومة أن الرواسب الرسوبية متموجة ومحكومة تركيبيًا داخل منطقة البحث. يُقدر أن يتراوح التدرج الحراري الأرضي وعمق خط كوري الحراري بين 19.10 و32.10 درجة مئوية/كم، وهذا لا يكفي لاستغلال الطاقة الحرارية الأرضية. وقد تمكّن البحث الحالي من تحديد المناطق النارية المتطفلة التي ينبغي تجنبها عند دراسة الهيدروكربونات. كما يُنتج نموذجًا يُسهّل تحديد التراكيب الجيولوجية المحتملة التي تتحكم في رواسب المعادن الخام المغناطيسية في المنطقة.

DOI: 10.33899/earth.2024.150856.1298, 

## Introduction

Geothermal energy is receiving increased attention from researchers and stakeholders as a result of the world's recent push to switch from fossil fuels to a more environmentally friendly and clean energy source. One renewable energy source that the nation may incorporate into its energy mix is geothermal energy because it is among the most affordable, available, abundant locally, and less polluting than conventional energy sources in Nigeria. It has the potential to contribute to Nigeria's energy goals. The Nigerian Government has partnered with other global governments to develop an energy roadmap aimed at augmenting the quantity of energy accessible for both industrial and residential use. This would be beneficial for examining the strategic energy plans and national energy policy, as well as for investors, consultants, and researchers looking to increase access to renewable energy sources in Nigeria for a range of uses. It will be of great importance if other alternative sources of energy are accessible to augment the energy sources already available in Nigeria. One sustainable way to add to the energy mix of the country is through geothermal exploration (Ikumbur et al., 2023).

Nigeria has the largest economy and the highest population on the African continent. Its population is among the fastest growing in the world, and as a result, demand for energy services, which are essential to enabling economic growth, is rising quickly (Usman et al. 2019). Since expanding access to clean, affordable energy is essential to development and

industrialization, this offers a significant opportunity to capitalize on the nation's abundant natural renewable energy resources and enable low-carbon growth. Nigeria's sources of renewable energy reveal that Nigeria has abundant natural renewable energy resources, which are crucial for the nation's sustainable development but now being severely underutilized. For example, two-thirds of the nation is covered by basement rock, but we are unable to access the area's crustal temperature potential (Emujakporue and Ekine, 2014). As a result, the area needs to be re-evaluated in order to potentially harness geothermal energy and incorporate it into the nation's energy mix. Water from hot springs has been utilized for bathing since the Paleolithic era and for space heating since the Roman era. More recently, however, geothermal energy has been investigated for the production of electricity (Ikumbur et al., 2023). In 2013, the anticipated amount of geothermal power accessible worldwide was 11,700 MW, and an extra 28 gigawatts of direct geothermal heating capacity was constructed for district heating purposes (Usman et al., 2023).

Magnetic materials, which are mostly found in basement rocks and less frequently in sedimentary strata, are the focus of aeromagnetic geophysical measurements. Anakwuba and Chinwuko (2015), Chinwuko et al. (2014), and Kivior et al. (1998) stated that new approaches such as ground gravity survey, borehole geophysical data analysis and radiometric methods are needed for subsurface exploration and that mapping the lithology and structure of the subsurface is a great opportunity provided by the magnetic method. This approach to target detection is quick, economical, and effective. When analyzing space data, like aeromagnetic, a spectrum analysis is particularly the useful method.

## Geology of the research area

The Bida Basin is an intracratonic basin that trends NW–SE and extends from the south of Lokoja to Kontagora in Niger State (Fig. 1a). Its boundaries include the Basement Complex in the northeast and southwest, and it merges with the Anambra and Sokoto basins in sedimentary fill made up of some thin unfolding marine sediments and post-orogenic molasses facies (Ojo and Akande, 2012). Among the principal lithologic units under investigation are the banded-gneiss, migmatite-gneiss, and granite-gneiss, all have clearly defined geologic limits. According to Obaje et al. (2004 and 2013), these rocks have experienced polycyclic deformation, which has resulted in the distortion of both micro and macro structures. The Southern Bida Basin is made up of the Lokoja Formation, which is layered on top of the Patti Formation, which is layered on top of the Agbaja ironstone Formation, according to Usman et al. (2023) (Fig. 1b). However, Ikumbur et al. (2013) have identified that the primary obstacle to hydrocarbon discovery in the Southern Bida Basin is the basin's fluctuating geothermal gradient. There is a chance that hydrocarbons will be found in the Southern Bida Basin, given the significant hydrocarbon accumulations that have been found in similar basins in African nations like Chad, Niger, and Sudan. Reevaluating the geology and hydrocarbon potential of the basin is therefore imperative.

The objective of this study is to analyze aeromagnetic anomalies across the Southern Bida Basin in order to identify regions that have high baseline temperatures and geothermal energy. By determining the Curie isotherm depth, common depth point and heat flow within the basin will aid in defining the basinal morphology. Additionally, the study will identify underlying structural features and may indicate areas that warrant additional research on the basin's geothermal energy generation.

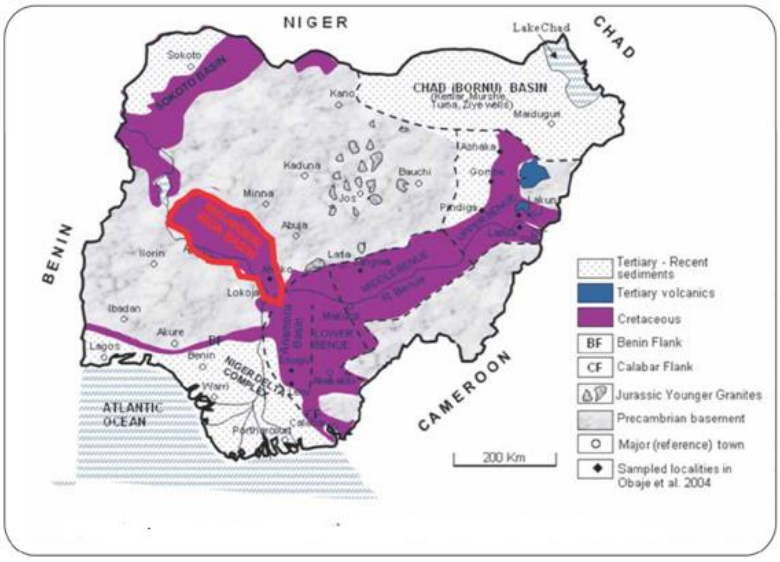


**Fig. 1a. Geological map of Nigeria and locations of the research region (After Usman *et al*., 2018).**

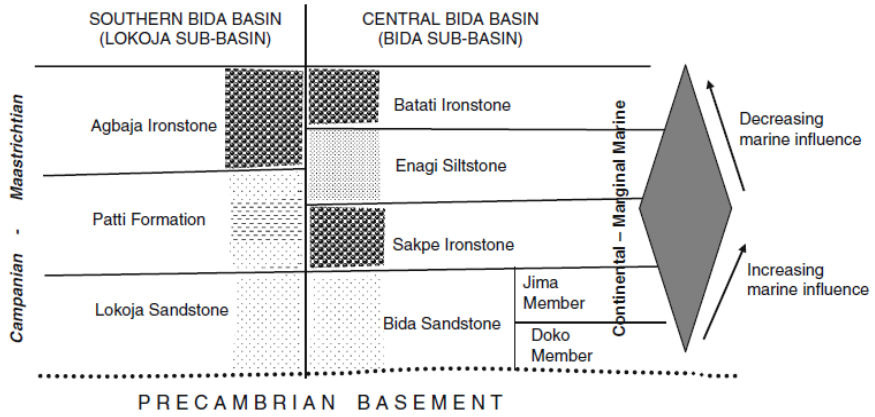


**Fig. 1b. Formation of southern Bida Basin correlated with Anambra Basin (modified from Akande et al., 2005).**

## Materials and Method

The Nigeria Geological Survey Agency (NGSA) provided the following nine aeromagnetic data, which were assembled and analyzed: Sheet 204 (Pateji), Sheet 205 (Baro), Sheet 206 (Gulu), Sheet 224 (Isanlu), Sheet 226 (Aiyegunle), Sheet 227 (Kotonkarifi), Sheet 234 (Ikole), Sheet 246 (Kabba), and Sheet 247 (Lokoja). The data were collected over a sequence of flight lines that run northwest–southeast at a distance of 2 km, with an average flight elevation of roughly 150 m. Tie lines were spaced approximately 20 km apart. The International Geomagnetic Reference Field (IGRF) was used to eliminate the geomagnetic gradient from the data. There are roughly 27,225 square kilometers covered in all. The nine acquired aeromagnetic maps were digitized at intervals of two kilometers along the flight lines. The intersection locations were then selected and contoured using contouring software (Oasis Montaj). The contoured anomalous magnetic data contains both local and regional anomalies (Fig. 2). A linear trend surface (Eq. 1) is generated and fitted onto the digitalized aeromagnetic total magnetic intensity (TMI) data to subtract the regional magnetic gradient from the residual anomaly data.

$$Z(x, y) = 1.1088x + 65.53y + 2512.029 \quad \ldots\ldots (1)$$

Where, Z= TMI at x and y; x = latitude value, y = longitude value.

Mathematical enhancement approaches are used to improve the magnetic data using both linear and non-linear algorithms in order to visually enhance the structural models (Biswas 2015; Bhattacharyya and Leu 1975; Odoh et al. 2021). We performed this improvement on our TMI data. Reduction to pole and regional residual separation are two of the filtering procedures, which is why initial vertical derivatives, are shown in figure (3). High-frequency magnetic responses are known to be correlated with high concentrations of mineral deposits (Odoh et al., 2021). In order to highlight the high frequencies and identifying the boundaries of the causal body, a high-pass filter and a horizontal gradient are added to the aeromagnetic data. The qualitative Euler Deconvolution method employing the Oasis Montaj software's Euler 3D extension came next (Abraham et al., 2023; and Bhattacharyya, 1966).

After conducting a spectral analysis of the data, the different depths to the magnetic source body are ascertained (Fig. 4a) from the running profile line in the residual anomaly map. Then, depth calculation is carried out using the Oasis Montaj software in steps as follows: The Fourier transform is used to generate the 2D Fourier transform analysis map (averaged energy spectrum), and the two depths are recorded and plotted using Surfer 11, and a combination of the shallow and the deeper magnetic basement source 3D model is accomplished. This is corroborated by Bensom et al. (2013); Chinwuko et al. (2014); Okonkwo et al. (2012 and 2021); Onwuemesi (1997); Bhattacharyya (1966); Spector and Grant (1970); and Usman et al. (2018 and 2023).

The following is a summary of the mathematical foundation of the spectrum analysis used in our in-depth calculation: Plotting the natural logarithm's amplitude ($a_n$) versus Nyquist frequency (n) (Eq. 2 and 3) resulted in Figure (4b). The power spectrum is used to determine each segment's slope, which is crucial information regarding the distance to the top of the causal body (Eq. 4 – 7) (Okubo et al., 1985) (Fig. 5). The Discrete Fourier Transform statement is found in equation:

$$\boldsymbol{Y_{i(x)}= \sum_{n=1}^{N} \left[ a_n \cos\left(\frac{2\pi n x_i}{L}\right) + b_n \sin\left(\frac{2\pi n x_i}{L}\right)\right]} \quad \ldots\ldots (2)$$

Where: $Y_i(x)$ = Reading at $x_i$ position
$L$ = Length (cross section) of the anomalous body
$n$ = harmonic number of the partial wave
$N$ = number of data points
$a_n$= real part of the amplitude spectrum
$b_n$= imaginary part of the amplitude spectrum
$i$ = 0, 1, 2, 3, ----------, n

**Partial Amplitude**

amplitude spectrum imaginary part

i = 0, 1, 2, 3, ----------, n

and,

$$\boldsymbol{a_n = \frac{2}{N} \sum_{i=1}^{N} Y_i \cos \frac{2\pi n x_i}{L}} \ldots\ldots (3)$$

$$\boldsymbol{b_n = \frac{2}{N} \sum_{i=1}^{N} Y_i \sin \frac{2\pi n x_i}{L}} \quad \textbf{..... (4)}$$

Usman et al. (2018) stated that the major amplitude spectrum ($A_n$) is as follows:

$$A_n = \sqrt{a_n^2 + b_n^2} \quad \text{..... (5)}$$

$$z = -ML/2\pi \quad \text{..... (6)}$$

Where, $z$ = depth to the basement ; $M$ = gradient of the linear segment

$L$ = width of the anomaly

The expression used to calculate the depth to centroid is provided by Nwankwo and Ekin (2010) corroborates this.

$$Z_b = 2Z_o - Z_t \quad \text{..... (7)}$$

The Euler deconvolution method is also deployed as an approach used in depth estimation that works best for anomalies caused by several independent anomalous sources. The structure index, or a measurement of the rate of change with distance from the field, is what meant to be represented by the homogeneity N (n in Euler's equation). A field that has an index of zero (zero) is always the same, independent of how far it is from the source model. A long profile of measurements could be divided into windows of consecutive measurements, and then subjected to the Euler approach, which can locate a simple body from magnetic field measurements. Next, a single estimate of depth and source location would be provided by each window.

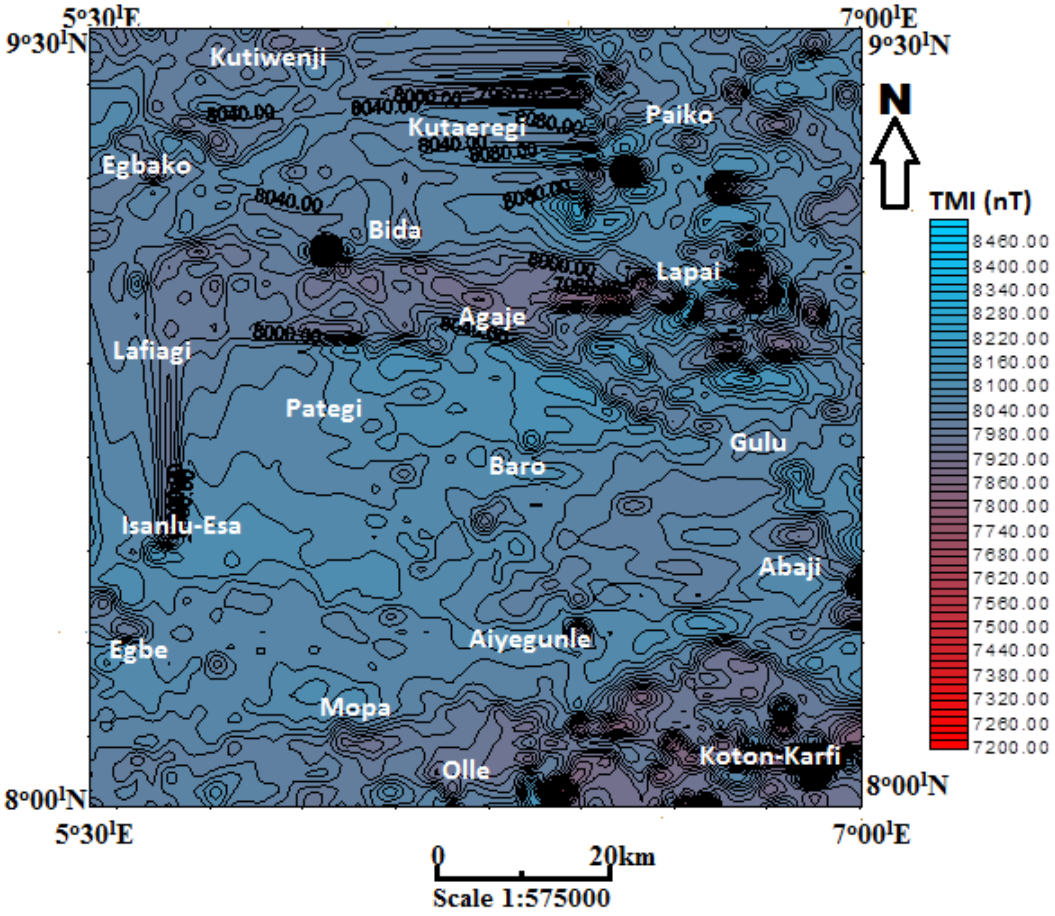


**Fig. 2. Total Magnetic Intensity (TMI) Map of the Southern Bida Basin (Contour Interval~20nT).**

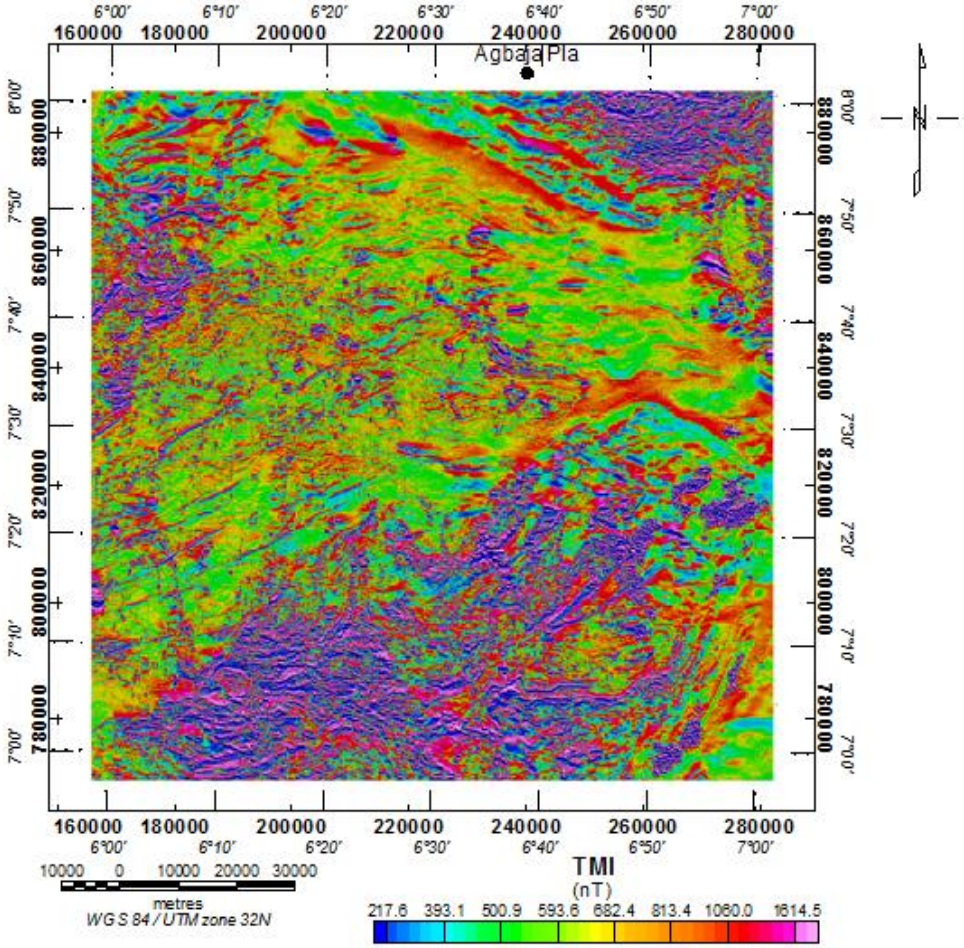


**Fig. 3. First Vertical Derivative (1VD) map of the research region.**

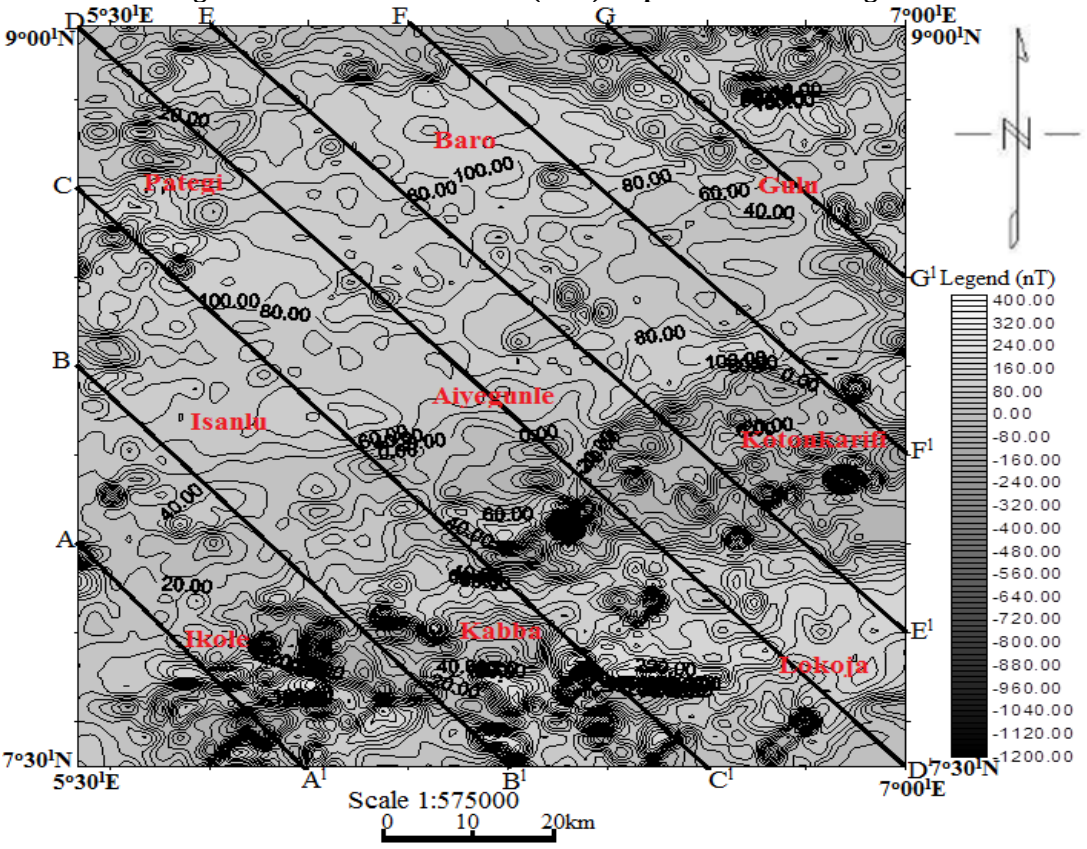


**Fig. 4a. Residual anomaly map with profiles taken perpendicular to the trend of the contours within the research region (Contour Interval ~20nT).**

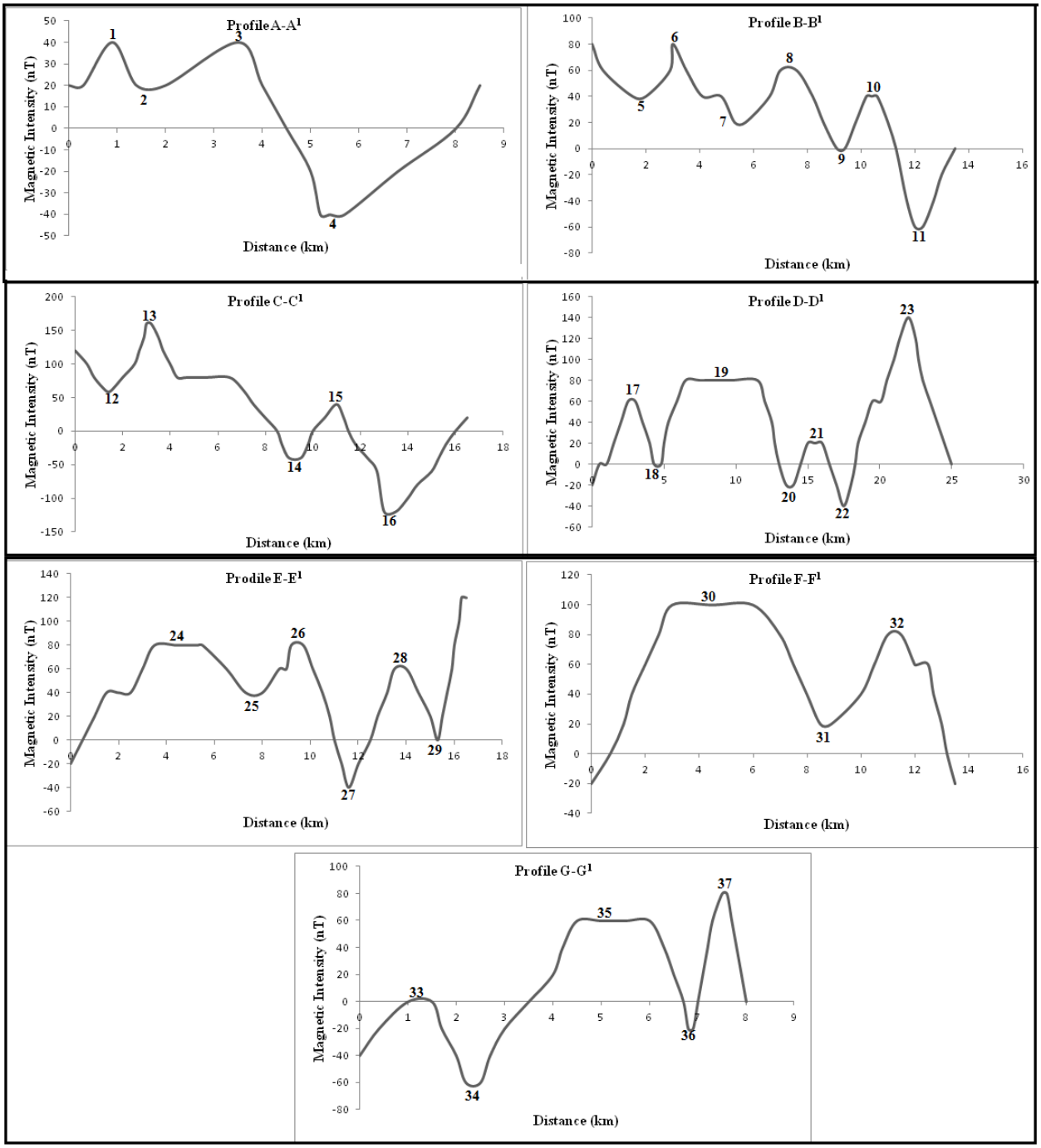


**Fig. 4b. Analysis from the trend profile line revealing the anomalous bodies.**

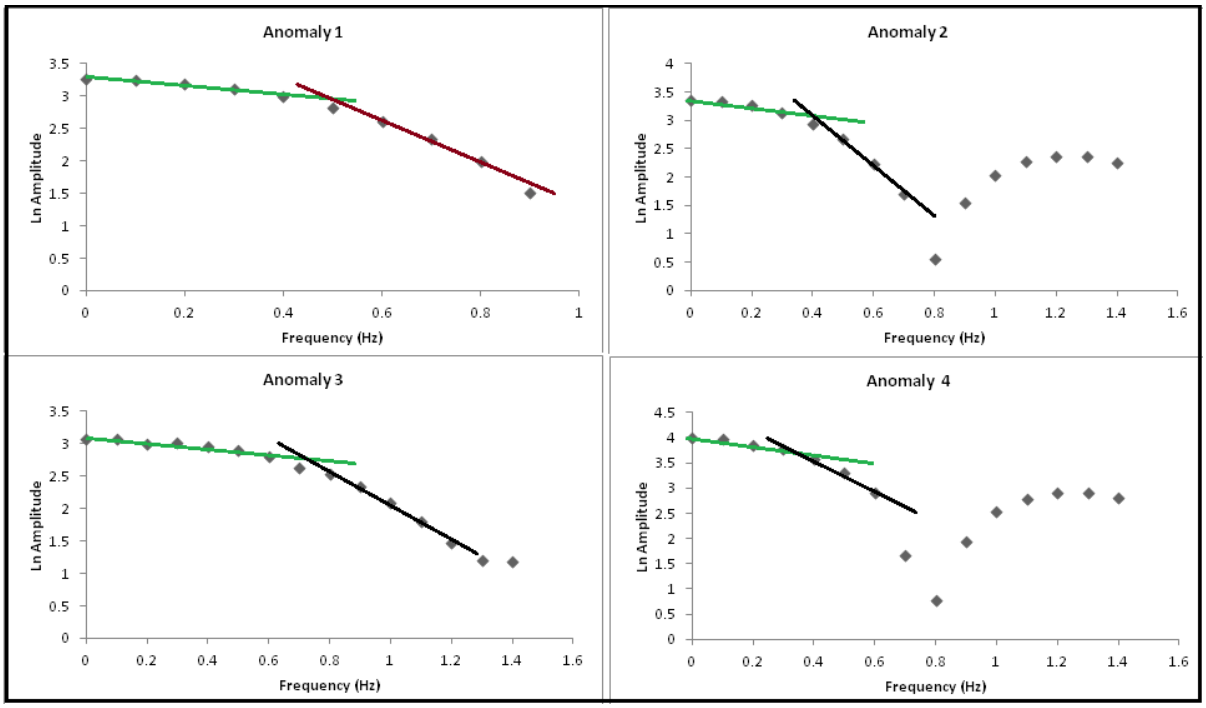


**Fig. 5. Spectral graph for Anomalies 1-4.**

## Results

Figures (2 and 4a) display the aeromagnetic maps of the research area's residual magnetic anomalies and total magnetic field strength. The residual anomalies and total magnetic field vary from -1200 to 400 nT and 7500 to 8800 nT, respectively, according to the maps. As a result, the maps display areas with low and high magnetization. They also demonstrate that there is significant evidence of higher magnetic intensity as well as a large number of anomalous bodies in the southeast portions of the Kotonkarifi axis, which comprise the Ikole-Kabba and Kotonkarifi intensities, respectively. Additionally, based on the visual interpretation, the closely spaced contour lines indicate that the basement depths surrounding these regions are quite shallow. Nonetheless, the contour lines in the center and northern regions (Isanlu, Aiyegunle, Pategi, Baro, and Gulu areas) are widely spread, indicating that the basement depths in these locations are rather high. The qualitative interpretation results also demonstrated that the region is severely faulted, with major faults going east-west (E-W) and smaller one's trending northeast-southwest (NE-SW) directions, based on visual inspection of the magnetic anomalies maps (Figs. 2, 3, and 4a).

The area's depth to the top (Zt) of anomalous bodies is identified by spectral analysis results (Fig. 6a). The lower sedimentary pill, which ranges from 0.45 to 1.49 km, is found around the south and southwestern regions of the research area (Kabba, Lokoja Ikole, and Kotonkarifi), and the higher sedimentary pill, which ranges from 1.81 to 3.24 km, is found in the northeast and southeast (Baro, Isanlu, Pategi, and Gulu regions) and is located in these regions (Fig. 6b). The analysis findings also demonstrate that the area's sedimentary thicknesses, or depths to the centroid ($Z_0$) and magnetic bodies, range from 9.09 to 16.84 km and 0.5 to 3.2 km, respectively. The Curie isotherm depth ranges from 16.0 to 23.0 km in the northwest (Figs. 7a and b), namely at the Isanlu and Pategi areas. In contrast, the other parts have deeper Curie isotherm depths (CPD), ranging from 24.0 to 32.0 km (Figs. 8a and b). In this location, the average depth of the Curie isotherm is 24.76 kilometers. The outcome additionally demonstrates that the Curie temperature isotherm inside the basin is an undulating surface rather than a level, horizontal surface. Geothermal gradients throughout the research region are produced by entering the values of Curie depth and Curie-point temperature (5800

°C) into equation 6 (Fig. 8 and Table 1). The obtained geothermal gradients have a range of 18.82 to 32.030 °C/km.

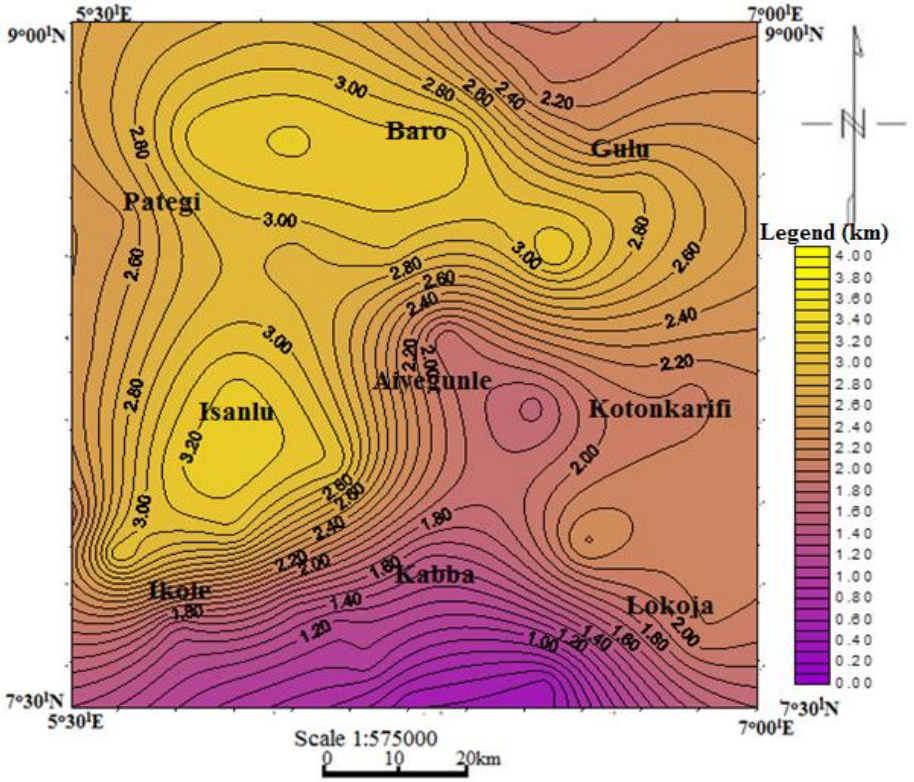


**Fig. 6a. Sedimentary pill thickness across the research area (Contour interval~ 1km).**

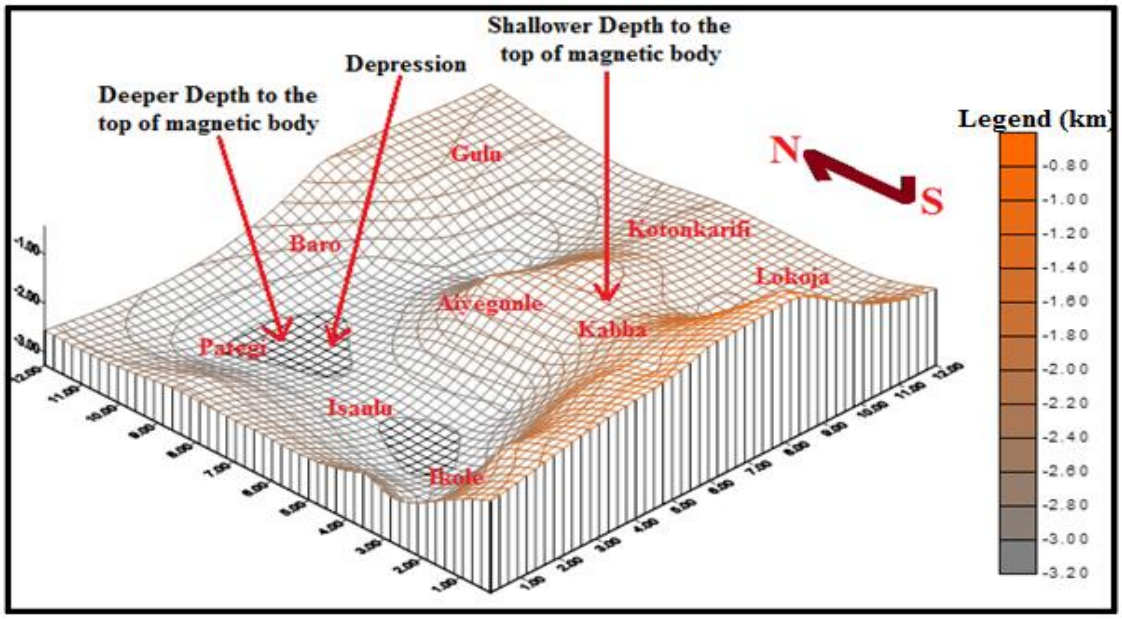


**Fig. 6b. Undulating basin morphology of the area.**

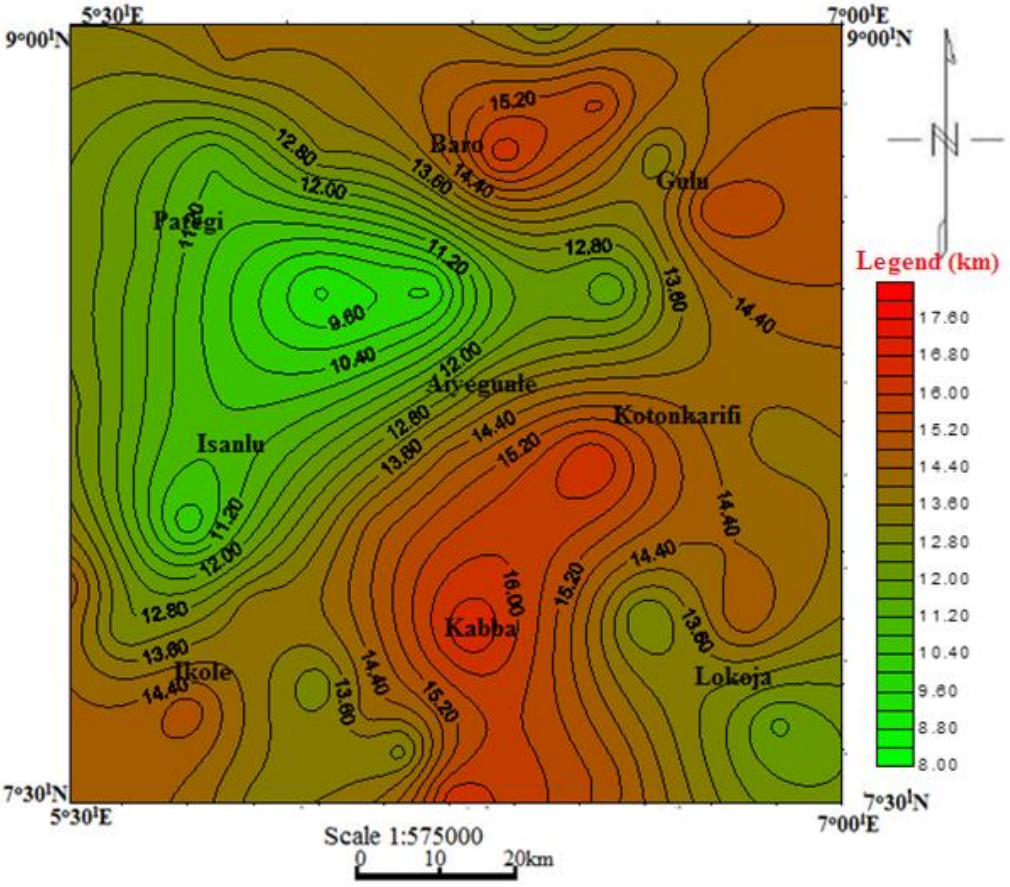


**Fig. 7a. Depth to centroid of the magnetic basement area (Contour interval~ 0.4km).**

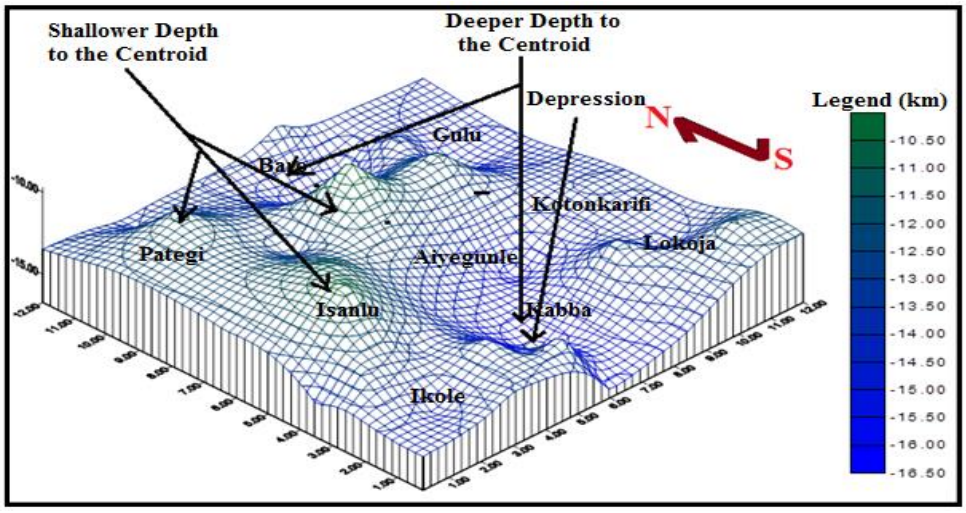


**Fig. 7b. 3D model view depth to centroid of the magnetic basement area.**

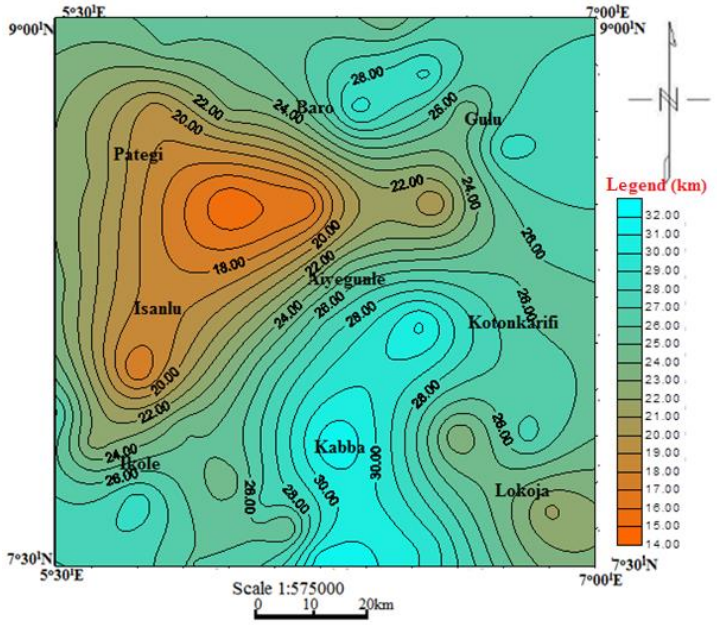


**Fig. 8a. Curie depth map of the research region (Contour interval~ 1.0km).**

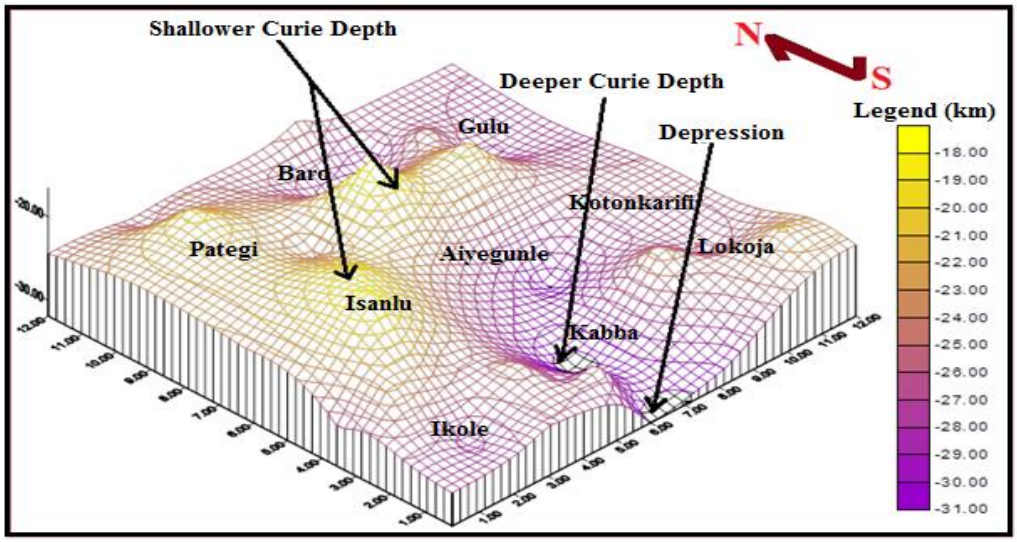


**Fig. 8b. 3D model view of Curie point depth of the research region.**

**Table 1: Estimation of depth to top ($Z_t$), depth of centroid ($Z_0$), Curie point depth (CPD), geothermal gradient and heat flow from spectral analysis.**

| Anomaly | $Z_t$ (km) | $Z_0$ (km) | CPD (km) | Geothermal gradient | Heat Flow(mWm2) |
|---|---|---|---|---|---|
| 1 | 2.09 | 14.73 | 27.37 | 20.1973 | 50.49324 |
| 2 | 3.11 | 12.84 | 22.57 | 24.49269 | 61.23172 |
| 3 | 1.49 | 15.11 | 28.73 | 19.24121 | 48.10303 |
| 4 | 0.96 | 13.45 | 25.94 | 21.31072 | 53.27679 |
| 5 | 2.42 | 12.88 | 23.34 | 23.68466 | 59.21165 |
| 6 | 3.18 | 10.06 | 16.94 | 32.63282 | 81.58205 |
| 7 | 3.05 | 13.92 | 24.79 | 22.29931 | 55.74829 |
| 8 | 1.52 | 12.87 | 24.22 | 22.82411 | 57.06028 |
| 9 | 1.14 | 14.31 | 27.48 | 20.11645 | 50.29112 |
| 10 | 1.08 | 12.95 | 24.82 | 22.27236 | 55.6809 |
| 11 | 0.53 | 16.28 | 32.03 | 17.25882 | 43.14705 |
| 12 | 2.46 | 12.21 | 21.96 | 25.17304 | 62.9326 |
| 13 | 3.22 | 11.04 | 18.86 | 29.31071 | 73.27678 |
| 14 | 3.07 | 14.53 | 25.99 | 21.26972 | 53.1743 |
| 15 | 1.49 | 16.84 | 32.19 | 17.17304 | 42.93259 |
| 16 | 0.45 | 15.06 | 29.67 | 18.63161 | 46.57904 |
| 17 | 2.71 | 13.01 | 23.31 | 23.71514 | 59.28786 |
| 18 | 3.24 | 9.09 | 14.94 | 37.00134 | 92.50335 |
| 19 | 3.19 | 11.23 | 19.27 | 28.68708 | 71.7177 |

| | | | | | |
|---|---|---|---|---|---|
| 20 | 2.85 | 13.69 | 24.53 | 22.53567 | 56.33918 |
| 21 | 2.25 | 14.47 | 26.69 | 20.71188 | 51.77969 |
| 22 | 2.33 | 12.61 | 22.89 | 24.15028 | 60.37571 |
| 23 | 2.08 | 11.89 | 21.7 | 25.47465 | 63.68664 |
| 24 | 2.86 | 14.05 | 25.24 | 21.90174 | 54.75436 |
| 25 | 3.23 | 13.11 | 22.99 | 24.04524 | 60.11309 |
| 26 | 2.98 | 9.47 | 15.96 | 34.63659 | 86.59148 |
| 27 | 1.81 | 13.22 | 24.63 | 22.44417 | 56.11043 |
| 28 | 1.65 | 16.51 | 31.37 | 17.62193 | 44.05483 |
| 29 | 2.13 | 14.83 | 27.53 | 20.07991 | 50.19978 |
| 30 | 3.17 | 16.32 | 29.47 | 18.75806 | 46.89515 |
| 31 | 3.22 | 11.63 | 20.04 | 27.58483 | 68.96208 |
| 32 | 2.08 | 13.83 | 25.58 | 21.61063 | 54.02658 |
| 33 | 2.01 | 12.94 | 23.87 | 23.15878 | 57.89694 |
| 34 | 2.14 | 15.77 | 29.4 | 18.80272 | 47.0068 |
| 35 | 2.33 | 13.22 | 24.11 | 22.92825 | 57.32061 |
| 36 | 2.79 | 15.64 | 28.49 | 19.4033 | 48.50825 |
| 37 | 2.47 | 14.85 | 27.23 | 20.30114 | 50.75285 |
| **Average** | **2.29135135** | **13.52594595** | **24.76054054** | **23.066** | **57.66499** |

## Discussion

This investigation has been conducted on the aeromagnetic anomalies over the Southern Bida Basin, Nigeria's Basement Complex, which makes room for some common invasive entities in some research area sections. In the meantime, the current investigation has been able to pinpoint the igneous intrusive zones that should be avoided when looking for hydrocarbons. The study also yields a model that makes it easier to identify possible locations for hydrocarbon accumulation and magnetic ore mineral deposits. Furthermore, the current study has offered a tool as an alternative, renewable, sustainable, and cleaner source of energy, the geothermal energy, for meeting human energy needs in order to reduce environmental pollution connected with the extraction and consumption of hydrocarbons in Nigeria.

The entire north-to-northeastern and southwestern portions of the map area clearly show indications of intrusion (Fig. 2). This accounts for the faulting and fracturing in the region. It was also thought that the Northeastern Nigerian Basement Complex outcropped inside and outside the research area, requiring the use of shallower sources that might include magnetic minerals and rocks (Wright et al., 1985). Furthermore, the magnetic patterns that have been detected (Fig. 3) show that the region has experienced complicated fracturing as a result of tectonic activity, with the major fault moving NE-SW and the minor fault trending SE-NW. These patterns match the architecture of the northern Nigerian region and the Basement Complex of the Benue Trough, and they could have functioned as a migration route for hydrocarbon or hydrothermal fluid in the studied area. Anakwuba and Chinwuko (2015) and Emujakporue and Ekine (2014) stated that areas with sediment infilling and substantially higher geothermal gradients will fall into the low oil window as opposed to areas with lower sedimentary thickness and gradient values. As a result, the northwestern side??? of the region (Isanlu, Pategi, and Aiyegunle) may be more conducive to petroleum accumulation. This is because they have relatively high sedimentary piles ranging from 1.81 to 3.24 km (Figs. 6a and 6b) and a geothermal gradient that ranges from 19.10 to 32.10 $^{o}$C/km. and this is not sufficient for geothermal energy exploitation (fig. 8 and Table 1) but the result compares favorably with the average geothermal gradient of 24.56 $^{o}$C/k. The average geothermal energy recorded in the region is 27.04.56 $^{o}$C/km within the Niger Delta, as reported by Emujakporue and Ekine (2014).

According to the results of the spectral analysis, there are two depth sources in the area. The shallower sources, which are located in the southeastern and southern regions (including Ikole, Kabba, Kotonkarifi, and Lokoja areas); and the deeper sources, which are located in the northwestern and northern regions (including Isanlu, Pategi, Baro, and Gulu areas) ranging from 0.45 to 1.49 km (Table 1). The analysis conclusion also reveals that the sedimentary thicknesses (depths to the centroid and magnetic bodies) range from 0.5 to 3.2 km and 9.09 to 16.84 km, respectively. The average depth of the Curie isotherm in the area is 24.76 km (Fig.

8). Once again, the correlation between the Curie depth isotherm and the geothermal gradient seems inverse (Fig. 10), which reveals that areas with a high geothermal gradient show a low Curie depth isotherm, which is shallower in the northwest part (specifically in the Isanlu and Pategi areas), with a Curie depth ranging from 16.01 to 22.98 km. At other parts, the Curie isotherm depth is deeper and ranges from 23.0 to 34.1 km. We advise that this area to be mapped for a detailed geothermal investigation due to the lack of temperature data in the region, despite the area's apparent promise. Since there is alot of fractures in the northeastern and southeastern regions, where these subsurface structures can operate as a channel for both geothermal and fluid migration. The region has low sedimentary infilling overall, but high curies isotherm depth indicates a big potential for mineralization. The region is undulating rather than having a horizontal surface as shown by the geological model (Figs. 11a–b). Additionally, it demonstrates that the sediments deposited in the study location is structurally controlled; figures 6b and 7b corroborate this assertion.

In order to particularly target various mapped sills and dike bodies within the study area, the Euler deconvolution result utilizing the structural index of 1 is employed. These structures have depth range values between 01 and 1917 m (Fig. 12). The classification of dykes, sills, and geological contacts as structures is crucial for the identification of mineralized zones. It is well known that different mineralized magmatic fluids (hydrothermal fluid) that form veins are deposited within the host rock's fracture and fault orifices during the magmatic emplacement and mineralization phases, whereas late-stage magmatic emplacement is rich in granitic rock content and is accompanied by high mineralization (Fig. 12). Zones of mineralization are linked to severe jointing and fractures. We focus on the localized mineralization and structures within our study area because, as Abraham et al. (2014) claimed, the structures are locally twisted in certain places, hiding the broader geology. There is a strong association between the different structures mapped using the vertical derivative map and the structures mapped using deconvolution and the SI of 0 and 1. This suggests that several of the primary targets are close to the surface and could serve as possible mineralization hosts. The outcome additionally demonstrates that the Curie temperature isotherm inside the basin is an undulating surface rather than a level, horizontal surface. Based on the computed sedimentary thicknesses (2.3–3.2 km), the geothermal gradient (18.82 and 32.03 $^{o}$C/km) (Fig. 9), and the fractures that may act as migratory pathways for hydrocarbon or hydrothermal fluid, there is a high likelihood of hydrocarbon generation in the northern and southeastern regions of the study area. The geothermal gradients across the study area range from 18.82 to 32.03 $^{o}$C/km.

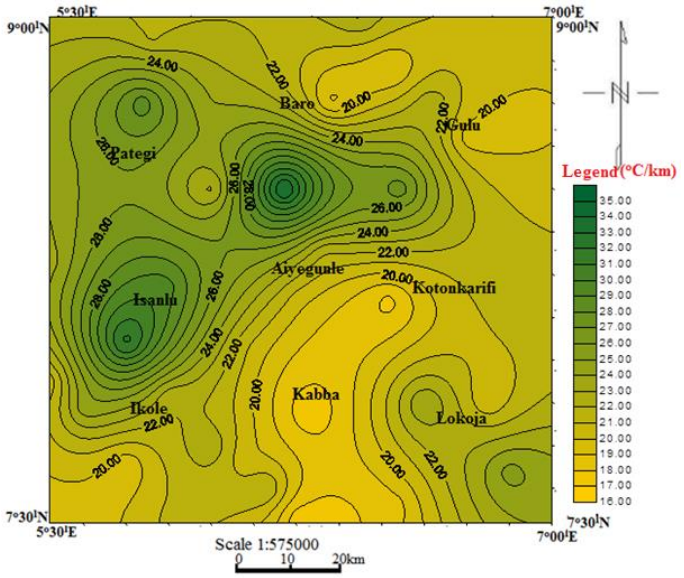


**Fig. 9. Map of geothermal gradient of the study area (Contour interval~ 1.0$^{o}$C/km).**

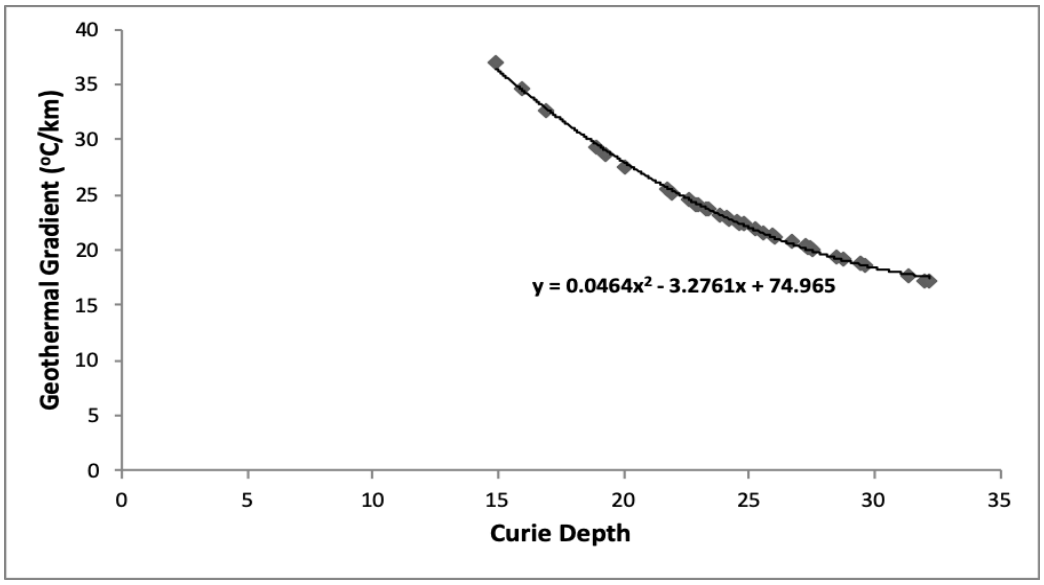


**Fig.10. Correlation between Curie depth and geothermal gradient within the study area.**

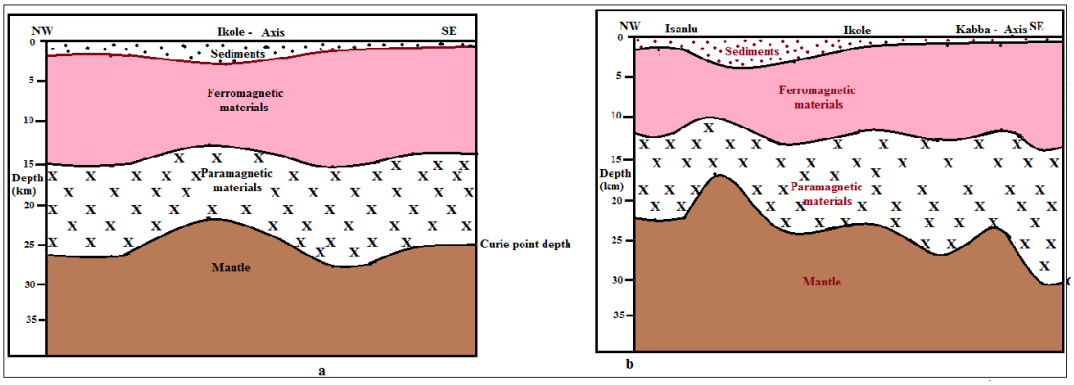


**Fig. 11. Curie point isotherm along profiles; (a) B-B1 and (b) D-D1.**

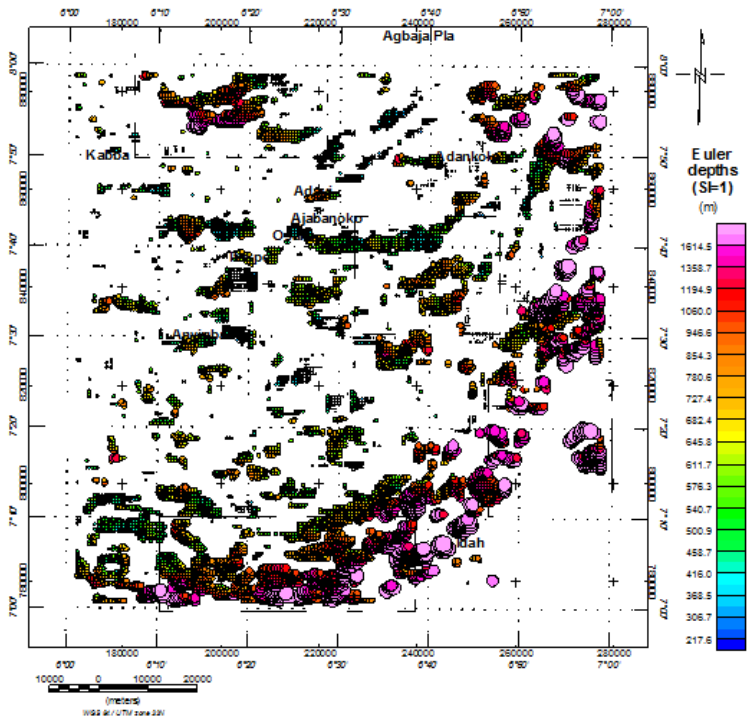


**Fig. 12. Magnetic field anomaly data with superimposed Euler solutions computed with a structural index of 1 to map various discordant and concordant structures within the area.**

## Conclusion

The geomagnetic dataset covering parts of the southern Bida basin has been re-evaluated, and the conclusions are as follows:

1. The researched region is greatly fractured, and the trend of the fracture is in the E-W direction. We conclude that the deeply seated structures in the region are conduits for both fluid and geothermal energy.
2. The results from the Euler convolution show that contact sources are delineated as dykes and sills. We believe that this structure controls mineralization in the region.
3. Spectral analysis results reveal two sedimentary pillars, with the thicker sedimentary infilling averaging 2.7 km, and an average geothermal gradient of 27.04 $^{o}$C/km. This region is recommended to be mapped out for a detailed geothermal energy study, while the region of lower sedimentary rock should be considered for mineral studies.
4. The 3D real-view models reveal that the sediment accumulation in the basin is undulating and structurally controlled.

## Acknowledgment

Our thanks go to TETFUND Nigeria for providing the Institutional Based Research Grant (with grant number: FUNAI/FS/BI/2020/015) used for this study.

## Conflict of interest Declaration

There is no conflict of interest in this research.

## References

Abraham, E., Usman, A., Chima, K., Azuoko, G. and Ikeazota, I., 2023. Magnetic Inversion Modeling of Subsurface Geologic Structures for Mineral Deposits Mapping in Southeastern Nigeria. Bulletin of the Mineral Research and Exploration, 1-1. https://doi.org/10.19111/bulletinofmre.1267876

Akande, S.O., Ojo, O.J. and Ladipo, K.O., 2005. Upper Cretaceous sequences in the Southern Bida Basin, Nigeria. Mosuro Publishers.

Anakwuba, E.K. and Chinwuko, A.I., 2015. One-Dimensional Spectral Analysis and Curie Depth Isotherm of Eastern Chad Basin, Nigeria. Journal of Natural Sciences Research, 5(19), pp. 14-22.

Biswas, A., 2015. Interpretation of Residual Gravity Anomaly Caused by a Simple Shaped Body Using Very Fast Simulated Annealing Global Optimization. Geoscience Frontiers, 6(6), pp. 875-893. DOI: 10.1016/j.gsf.2015.03.001

Bhattacharyya, B.K., 1966. Continuous Spectrum of the Magnetic Field Anomaly due to a Rectangular Prismatic Body. Geophysics, 31, 121. http://dx.doi.org/10.1190/1.1439767

Bhattacharyya, B.K., and Leu, L.K., 1975. Spectral Analysis of Gravity and Magnetic Anomalies due to Two-Dimensional Structures. Geophysics, 40, 993-1003. https://doi.org/10.1190/1.1440593

Bemsen, I.E., Onwuemesi, A.G., Anakwuba, E.K., Chinwuko, A.I., Usman, A.O. and Okonkwo, C.C., 2013. Spectral Analysis of Aeromagnetic Data Over Part of the Southern Bida Basin, West-Central Nigeria. International Journal of Fundamental Physical Sciences, 3(2), pp. 27-31. DOI: 10.14331/ijfps.2013.330050

Chinwuko, A.I., Usman, A.O., Onwuemesi, A.G., Anakwuba, E.K., Okonkwo, C.C. and Ikumbur, E.B., 2014. Interpretations of Aeromagnetic Data Over Lokoja and Environs, Nigeria. International Journal of Advanced Geosciences, 2(2), pp. 66-71. DOI: 10.14419/ijag.v2i2.2305

Emujakporue, G.O. and Ekine, A.S., 2014. Determination of Geothermal Gradient in the Eastern Niger Delta Sedimentary Basin from Bottom Hole Temperatures. Journal of Earth Sciences and Geotechnical Engineering, 4(3), pp. 109-114.

Ikumbur, E.B., Onwuemesi, A.G., Anakwuba, E.K., Chinwuko, A.I. and Usman, A.O., 2023. Evaluation of Geothermal Energy Potential of Parts of the Middle Benue Trough Nigeria: Aeromagnetic and aeroradiometric approach. Iranian Journal of Geophysics, 16(4), pp. 7-52. DOI: 10.30499/ijg.2022.295242.1343

Ikumbur, E.B., Onwuemesi, A.G., Anakwuba, E.K., Chinwuko, A.I. and Usman, A.O., 2013. Spectral Analysis of Aeromagnetic Data Over Part of the Southern Bida Basin, West-Central Nigeria. International Journal of Fundamental Physical Sciences, 3(2), pp. 27-31. DOI: 10.14331/ijfps.2013.330050

Kivior, I. and Boyd, D., 1998. Interpretation of the Aeromagnetic Experimental Survey in the Eromanga/Cooper Basin. Canadian Journal of Exploration Geophysics, 34(1), pp. 58-66.

Nwankwo, C.N. and Ekine, A. S., 2010. Geothermal gradients in the Chad Basin, Nigeria, from bottom hole temperature logs. Scientia Africana, 9(1), 37-45.

Obaje, N. G., Wehner, H., Hamza, H. and Scheeder, G., 2004. New Geochemical Data from the Nigerian Sector of the Chad Basin: Implications on Hydrocarbon Prospectivity. Journal of African Earth Sciences, 38(5), pp. 477-487. https://doi.org/10.1016/j.jafrearsci.2004.03.003

Obaje, N.G., et al., 2013. Preliminary Integrated Hydrocarbon Prospectivity Evaluation of the Bida Basin in North Central Nigeria. An International Journal, 3(2), pp. 36-65.

Odoh, O.P., Ezeh, C.C., Usman, A.O., Okanya, O.S. and Chima, C.J., 2021. Delineation of Basin Geometry Within Parts of Northern Anambra Basin, Nigeria: An aeromagnetic approach. Journal of Environment and Earth Science, 11(4), pp. 28-39. DOI: 10.7176/JEES/11-4-04

Ojo, O.J. and Akande, S.O., 2012. Sedimentary Facies Relationships and Depositional Environments of the Maastrichtian Enagi Formation, Northern Bida Basin, Nigeria. Journal of Geography and Geology, 4(1), pp. 136-147. DOI:10.5539/jgg.v4n1p136

Okonkwo, C.C., Onwuemesi, A.G., Anakwuba, E.K., Chinwuko, A. ., Okeke, S.O. and Usman, A.O., 2021. Evaluation of Thermomagnetic Properties and Geothermal Energy Potential in parts of Bida Basin, Nigeria, using spectral analysis. Bulletin of the Mineral Research and Exploration, 165, pp. 13-30.https://doi.org/10.19111/bulletinofmre.796381

Okubo, Y.J., Graf, R., Hansen, R.O., Ogawa, K. and Tsu, H., 1985. Curie Point Depth of the Island of Kyushu and Surrounding Areas. Japan Geophysics, 53, pp. 481-491. https://doi.org/10.1190/1.1441926

Onwuemesi, A.G., 1997. One-Dimensional Spectral Analysis of Aeromagnetic Anomalies and Curie Depth Isotherm in the Anambra Basin of Nigeria. Journal of Geodynamics, 23(2), pp. 95-107. https://doi.org/10.1016/S0264-3707(96)00028-2

Spector, A. and Grant, F.S., 1970. Statistical Models for Interpretation of Aeromagnetic Data. Geophysics, 35, pp. 293-302. https://doi.org/10.1190/1.1440092

Usman, A.O., Ezeh, C.C. and Chinwuko, I.A., 2018. Integration of Aeromagnetic Interpretation and Induced Polarization Methods in Delineating Mineral Deposits and Basement Configuration Within Southern Bida Basin, North-West Nigeria. Journal of Geology and Geophysics, 7, 449.

Usman, A.O., Ezeh, C.C. and Chinwuko, A.I., 2019. Estimation of Geothermal Gradient and Curie Point Depth for Delineating Hydrocarbon Potential Zones Over Southern Bida Basin, Northwestern Nigeria. Development Journal of Science and Technology Research, 8(1), pp. 105-119.

Usman, A.O., Chinwuko, A.I., Azuoko, G.B., Ekwe, A.C., Abraham, E.M. and Chizoba, C.J., 2023. Geomorphological Mapping of the Basin Configuration of Parts of Southern Nupe Basin, Nigeria, Using High-Resolution Aeromagnetic and Core Drill Dataset. Iranian Journal of Geophysics.

Wright, J.B., Hastings, D., Jones, W.B. and William, H.R., 1985. Geology and Mineral Resources of West Africa. George Allen and Unwin London, England